

RESEARCH ARTICLE

Omni-wheel friction coefficient measuring methodology for various angles

Vlad Petrescu^{*†}, Aleksandar Petrov[†], Isabelle El-Hajj[†], Raf van Son[‡] and Derek Gransden[†]

Abstract

Omni-wheels are more and more used in robotics. As the friction coefficient of the wheels is one of their important design parameters, there is an arising need for techniques for obtaining this value. This paper presents a friction coefficient measurement technique for omni-wheels. The designed set-up involves placing an omni-wheel specimen on a shaft that allows for varying the angle between the direction of movement and the rolling direction. When torque is applied on the shaft, the wheel is moving a contact surface which is constrained to translate in a single direction. A pair of strain gauges is attached to the shaft in order to measure the shear strain which is related to the torque and therefore, to the friction force. The slip ratio was obtained from readings of the angular position of the wheel and the displacement of the contact surface. In order to verify the set-up, a 10 cm diameter omni-wheel was tested on an artificial grass surface at four different angles (0° , 15° , 30° and 45°), between 40 and 80 N as normal weight. The measurement technique proved to be valid and effective. It was also observed that the values of the coefficient of friction showed dependency on the angle between the direction of movement and the rolling direction.

Keywords: omni-wheel; friction coefficient; measure; slip ratio

Background

Omni-wheels are used to a great extent in robotic applications. They have a number of small rubber rollers that can turn perpendicular to the wheel rotating direction (see Fig. 1). Therefore, they can be driven in one direction while sliding in another. For this reason, motion platforms utilising omni-wheels can be designed in a way that does not require steering. That is why, they are commonly used in competitions such as Robocup or FIRST Robotics. In these events, robots need to be optimized with respect to weight and speed. Therefore, in such applications omni-wheels often perform at friction coefficient values close to the maximum static value. Consequently, the knowledge about this value and its dependence on approach angle (the angle between the direction of translation of the wheel and the rolling direction) is of utmost importance for the design of the motion platform of these robots. Therefore, the current research focuses on the development of a methodology for obtaining the value of the maximum static friction coefficient at various approach angles.

Modelling the frictional interaction between an omni-wheel and an elastic or elastomeric surface is complicated due to the complex physical processes. For this reason, a theoretical model has not yet been developed. Even the most basic approach, namely the Coulomb friction model, presents complications. It states that there exists a friction coefficient μ that is constant for any pair of materials and that equals the ratio between shear (τ) and normal (σ) stresses at the interface between the two objects (see Eqn. 1).

$$\mu = \frac{\sigma}{\tau} \quad (1)$$

The friction coefficient obtained from the Coulomb model deviates from reality as it depends on the contact time, normal force and sliding speed [1]. Furthermore, due to the irregularity of surfaces at the interface between two bodies, the real contact area is smaller than the apparent area [2]. Although for many materials the real contact area approaches the apparent area as the normal force increases, the effect of saturation leads to real contact being smaller than the apparent area regardless of the normal force applied for elastomers such as rubber [3]. The saturation effect influences both the shear and normal stress distributions

*Correspondence: petrescv@gmail.com

Full list of author information is available at the end of the article

[†]Faculty of Aerospace Engineering, Delft University of Technology

[‡]Falcons team, ASML B.V.

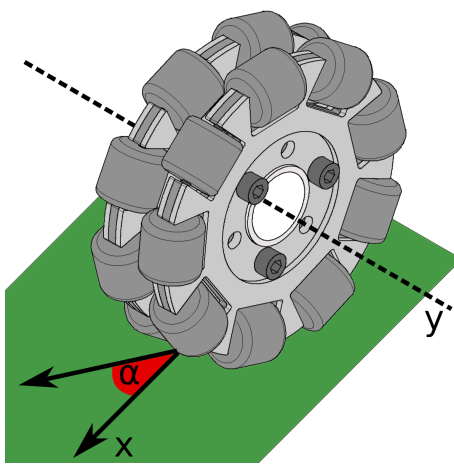


Figure 1 Illustration of an omni-wheel. The rolling direction can be seen (coincident with the x -direction). The direction of movement and the angle α between it and the rolling direction are also shown

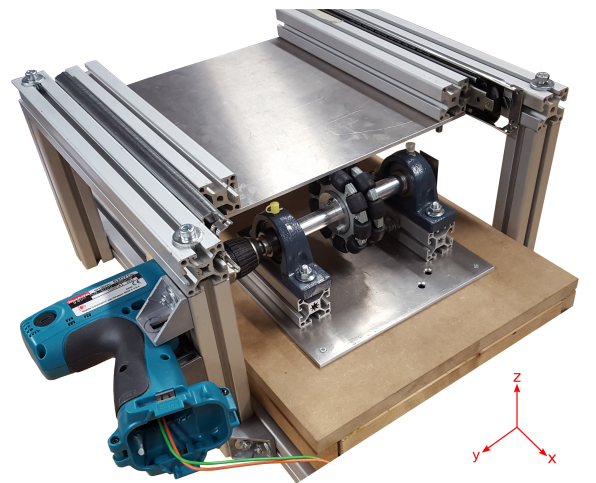


Figure 2 Illustration of the test set-up. The contact material is attached between the upper aluminum plate and the omni-wheel

at the interface between the bodies. Therefore, an accurate model of the stress distributions is critical for an investigation of the frictional interaction.

A more elaborate approach includes the deformation of the omni-wheel rollers and the surface. In this case the frictional interaction is even more complex. Goryacheva presents the modern tribological view of the causes of the rolling contact resistance as two-sided: adhesive component and mechanical component. The adhesive component follows the Coulomb model but with an offset τ_0 (see Eqn. 2). For polymers τ_0 is very small and can be neglected [3].

$$\tau = \tau_0 + \mu\sigma \quad (2)$$

On the other hand, the mechanical component of the rolling contact resistance accounts for energy loss due to the repetitive deformation and restoration of the rollers. Elastic bodies do not dissipate energy during deformation and restoration. Therefore, the mechanical component of the rolling contact resistance of the elastic bodies is zero. However, due to hysteresis, viscoelastic bodies experience inelastic deformations and thus, witness energy losses [3]. As the rollers of an omni-wheel are made out of rubber, its contact interaction is in essence viscoelastic. For this reason, the mechanical component of the rolling resistance of an omni-wheel cannot be neglected.

Due to the deformation at the interface between the two bodies, pure rolling cannot occur. Instead, there are regions of partial slip that contribute significantly to the rolling resistance [4]. The slip and the overall deformation of the outer surface of the cylinder

lead to the circumferential speed of the roller differing from the translational speed [1]. This difference can be quantified as

$$s = \frac{\omega R - V}{V}, \quad (3)$$

where the quantity s is called *creep ratio* or *slip ratio*, V denotes the translational speed, ω is the rotational speed of the cylinder and R is its radius.

Analytical models for viscous or rigid rollers on a viscoelastic half-space taking into account the effects discussed so far have been developed by multiple researchers [3, 5, 6]. Nonetheless, these models are relatively limited in their flexibility and cannot be adapted for a complex mechanism as an omni-wheel. That is why only a numerical FEM or an experimental approach is applicable for this case. In the current paper, the experimental aspect of this problem is investigated.

However, to current knowledge, systematic experimental methodology allowing testing of an omni-wheel at different approach angles does not exist. Many tire friction measuring systems exist. For example, the SRT-4 measurement system [7] is able to acquire information on the road surface adhesion using a tire attached to a dynamometer trailer. Also, the U.S. Department of Transportation is performing tests on tire rolling resistance [8] by substituting the contact surface with a wheel whose radius is significantly larger than that of the specimen. Still, none of these approaches can be directly applied to an omni-wheel that is not aligned with the direction of motion.

That is why, the goal of this research is to develop equipment for measuring the friction coefficient of an

omni-wheel at various angles. The test frame has a moving platform that is in contact with the wheel (see Fig. 2). By applying torque to the wheel, the platform moves and its displacement is recorded. The rotational displacement of the wheel together with the normal force and the applied torque are also recorded. The data is then processed such that a single value for the friction coefficient is obtained for each test run. The novelty of the approach described in this paper is that it allows for testing at different approach angles. The results show that the friction coefficient of an omni-wheel in contact with an artificial grass surface depends on the approach angle. It was demonstrated that the coefficient of friction is increasing with this angle.

Methods

Specimens

Two omni-wheels were used to validate the test set-up. The original (clean) omni-wheel is presented in Fig. 1 and it has nine rubber rollers on each of its two sides. The rim is made out of aluminum and allows the rollers to rotate independently, on bearings, around their axes. The wheel weighs 0.3 kg, is 10 cm in diameter and has a mass moment of inertia of $4 \text{ kg}\cdot\text{cm}^2$ around the axis of rotation. The second (coated) omni-wheel is identical to the original one, but with an extra coating on the rollers. The ECO Profi-Allgrund (Delta Lackcolor) mixed with anti-slip powder (Epifanes) was applied.

Mechanical set-up

As illustrated in Fig. 2, the set-up consists of 40 mm square profile aluminum frame and is composed of a fixed and a moving platform. The latter is free to slide in the x direction, as it is supported on rails. On the platform, the contact material is attached between the aluminum plate and the wheel. The static part consists of the base on which the shaft and the wheel are attached by two bearings. When torque is exerted on the shaft, the wheel can rotate around the y -axis and therefore translate the contact surface in the x direction.

The base offers support for attaching the bearings at four different locations. This enables the shaft to be rotated in the xy -plane in four steps: 0° , 15° , 30° and 45° with respect to the forward movement (x -axis). In this way, the friction coefficient of the omni-wheel can be tested at different approach angles. The entire structure of the base is supported on an electronic scale which measures the normal force during testing. Because the moving platform is attached with bolts on the four vertical struts, the normal weight experienced by the wheel can be varied between 40 N and 80 N.

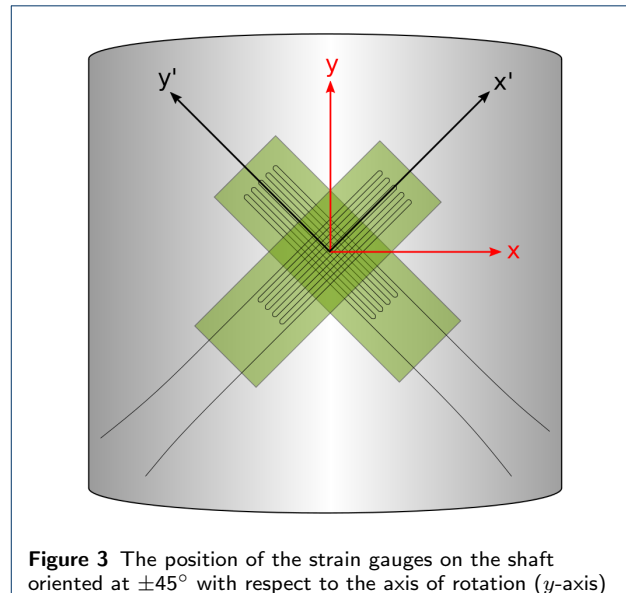


Figure 3 The position of the strain gauges on the shaft oriented at $\pm 45^\circ$ with respect to the axis of rotation (y -axis)

The movement in the x -axis and the angular displacement of the wheel are recorded by two potentiometers attached to the rotating shaft and to a pulley, respectively. By measuring the resistance across the potentiometer attached to the shaft, the angular rotation of the wheel can be found, as the relation is proportional. In a similar way, the displacement in the x -axis can be measured. A thread is attached and wound at one end on the on pulley and at the other end on the moving platform.

The torque experienced by the shaft is exerted by a 10 V DC motor and a gearbox assembly mechanism. This is able to supply with up to 13 Nm at the shaft, depending on the input power. The latter can be varied using a voltage regulator.

In order to measure the friction coefficient during a dynamic test, the applied torque on the shaft is to be measured. This is done by using a pair of strain gauges placed on the shaft at $\pm 45^\circ$ with respect to the axis of the shaft (see Fig. 3). According to Saint-Venant's principle [9], the strain should be measured at a distance of more than two diameters away from the clamping zones. This is why, the strain gauges are placed at a significantly large distance from the motor or the wheel (see Fig. 4).

Control and data acquisition

The control of the system and the data recording was done by a personal computer via a National Instruments USB6009 Data Acquisition System (DAQ). The resistance changes in the strain gauges resulting from the applied torque were too small to be measured by the DAQ. That is why a PICAS amplifier (Peekel

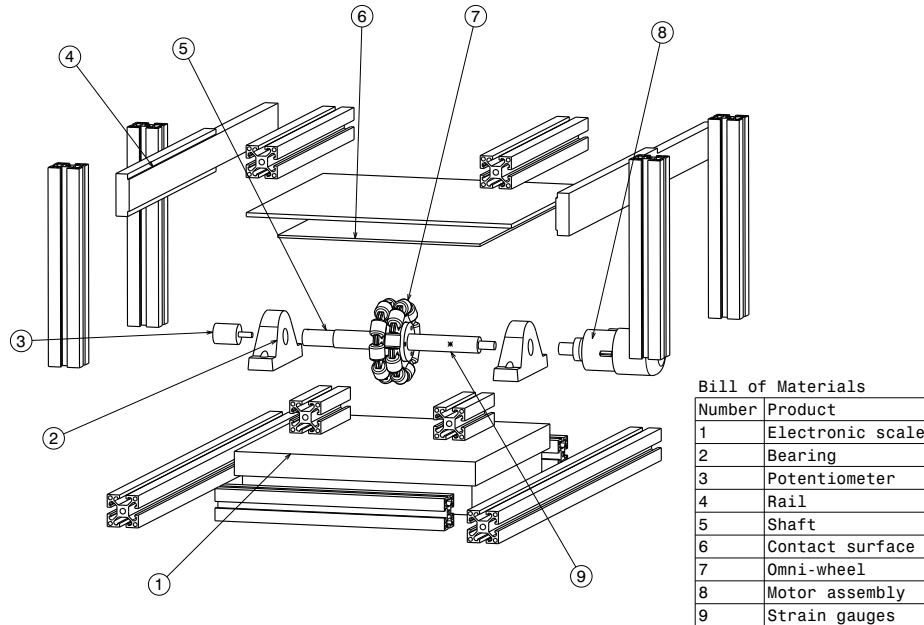


Figure 4 Exploded view of the test set-up drawing

Instruments) was used. This instrument individually amplified the two strain gauge signals using a Wheatstone bridge [10]. The amplified voltages were sent to the DAQ via two analog coaxial outputs of the PICAS. The readings of the two potentiometers were directly sent to the DAQ. Additionally, an output channel of the DAQ was connected to a normally open relay that was used to turn on the motor.

Custom-made software was used to record the data and control the testing equipment (see Fig. 5). The user interface of this software allowed for inspecting the current readings of the potentiometers and the strain gauges, starting and stopping the motor and recording the acquired data. Furthermore, at the end of each test run, it displayed the strain gauge voltages and potentiometer readings. During a test run, the software recorded the data from all channels simultaneously at a frequency of 9600 Hz. The normal force measured by the scale was manually entered in the software before the start of each run test due to its low update rate.

As the duration of each test run was less than 0.7 seconds, manual cutting of the power to the motor was not feasible. That is why, in parallel with the data recording, the software monitored the readings of the potentiometers and stopped the test automatically when the platform had moved to its furthest position. Even though ten revolution potentiometers

were used, automatic stopping was also incorporated in order to prevent damage to the equipment.

Torque measurements

The measured torque was used to determine the friction force experienced by the omni-wheel during a test run. First, the signals from the strain gauges were smoothed. Then, by using a number of stress and strain transformations, torque as a function of test time was obtained. Finally, a single representative torque value was determined.

Stress and strain transformations The shear strain γ_{xy} can be computed as a result from the two strain gauge measurements, ε_x' and ε_y' , positioned according to Fig. 3. Evaluating the following two equations [11]

$$\begin{aligned}\varepsilon_x' &= \varepsilon_x \cos^2 \theta + \varepsilon_y \sin^2 \theta + \gamma_{xy} \cos \theta \sin \theta \\ \varepsilon_y' &= \varepsilon_x \sin^2 \theta + \varepsilon_y \cos^2 \theta + \gamma_{xy} \cos \theta \sin \theta\end{aligned}\quad (4)$$

at $\theta = 45^\circ$ (the rotation angle between x-y and x'-y' axis systems) and by subtracting one from the other, the shear strain γ_{xy} is as follows:

$$\gamma_{xy} = \varepsilon_x' - \varepsilon_y'. \quad (5)$$

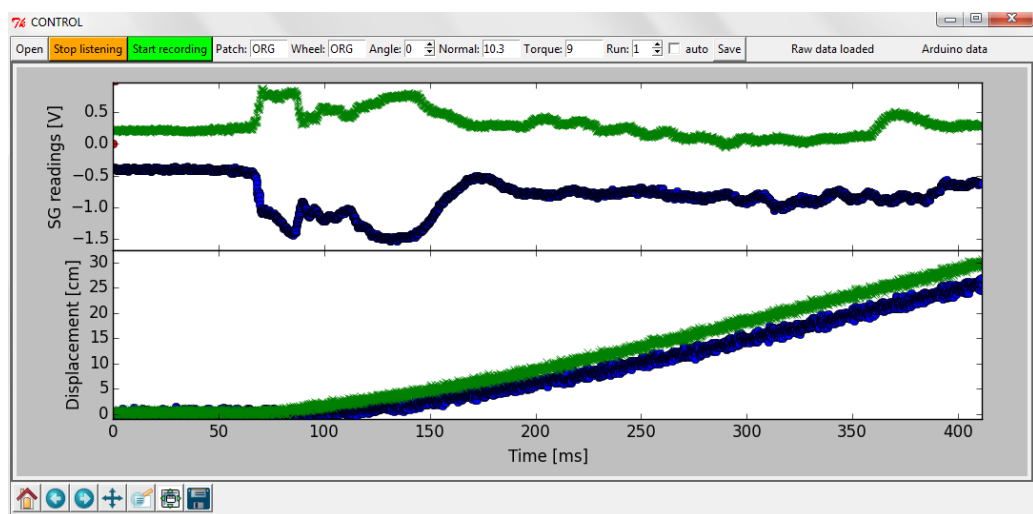


Figure 5 Software control panel

Once the shear strain is known, the torque T can be computed using linear elastic mechanics:

$$T = \frac{\gamma_{xy} J G}{R}, \quad (6)$$

with R and JG being the radius and the torsional rigidity of the shaft, respectively. As it is made out of aluminum type 6082, the shaft has a G of 26 GPa. With a 10 mm radius, J is found to be 1.6 cm⁴.

The calibration of the instruments was performed by applying a constant torque on the shaft. The latter was clamped in the middle, at the position of the wheel. Torque was applied at one end of the shaft using a moment arm. A 3 kg weight was pulling down the arm, torquing the shaft with 6 Nm. As the described calibration did not exert only a pure torque but induced also a bending on the shaft about the x -axis, corrections were implemented using Eqn. 4. In that way the exact value of the torsional rigidity was obtained.

Fourier series fitting Due to noisy measurements, the readings for the two strain gauges had to be smoothed before applying the stress and strain transformations described in the previous section. The recorded strain gauge voltage signals were of oscillatory nature. For this reason, it was decided to use the least squares method to fit measurements to a Fourier series. Choosing only high frequency Fourier terms in the fitting function, had the effect of applying a low pass filter. In particular, only terms with frequencies from 0 to 19 Hz were used as this gave a good noise reduction to feature loss ratio. It shall be noted that the 0 Hz term equals the average of the signal. It was

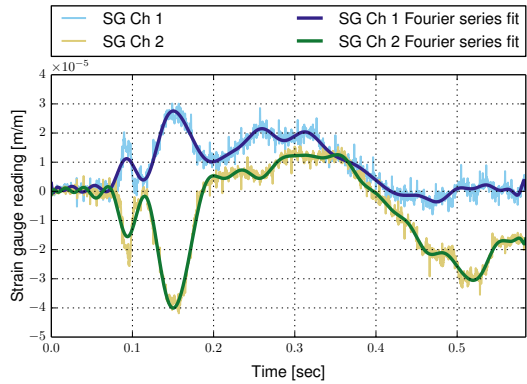


Figure 6 Illustration of the Fourier fitting procedure at $N = 19$ for the recorded readings of the two strain gauges

decided to use frequencies based on fractions of 1 sec instead of frequencies based on fraction of the test run duration. In this way, the potential operations of signals from different runs, with different durations, could be facilitated.

The fitting function f is:

$$f = \sum_{n=0}^N a_n \cos(2\pi nt) + b_n \sin(2\pi nt), \quad (7)$$

where, in this case, N was set to be 19 and t is the time since the start of the test run. The coefficients $a_0, \dots, a_N, b_0, \dots, b_N$ should be chosen such that the sum of the squared residuals of each strain gauge voltage measurement is minimized. The problem of finding the coefficient vector $\mathbf{c} = [a_0, b_0, \dots, a_N, b_N]^T$ reduces

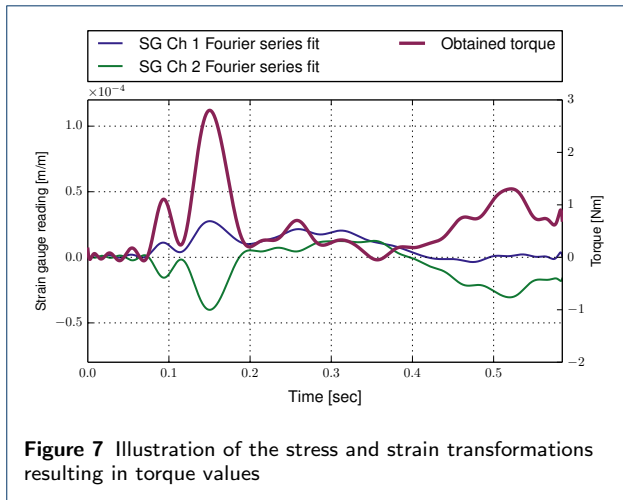


Figure 7 Illustration of the stress and strain transformations resulting in torque values

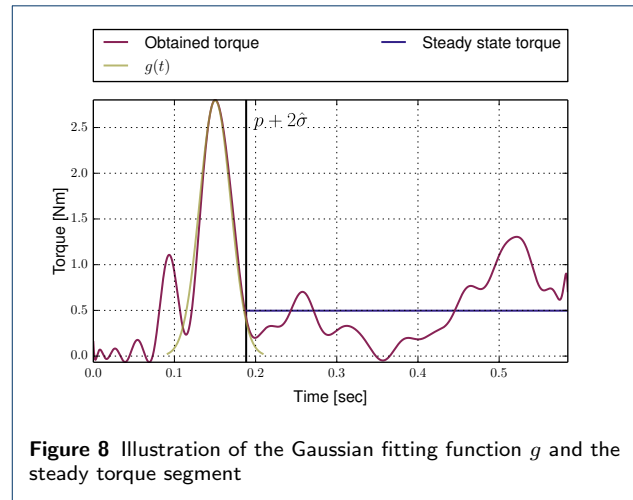


Figure 8 Illustration of the Gaussian fitting function g and the steady state torque segment

to obtaining the least squares solution of the following inconsistent system:

$$\begin{aligned} \mathbf{A}\mathbf{c} &= \mathbf{y}, \\ A_{i,2k+1} &= \cos(2\pi kt_i), A_{i,2k+2} = \sin(2\pi kt_i) \quad (8) \\ \text{for } k &= 0, \dots, N, i = 0, \dots, M. \end{aligned}$$

In Eqn. 8, \mathbf{y} is a vector of length M holding the voltage measurements for a given channel. Time t_i is the time in seconds since starting the test run at which voltage measurement y_i was taken. Note that coefficient b_0 is unnecessary and is kept only for consistency. The results of the Fourier series fitting procedure are illustrated in Fig. 6.

The operations for stress and strain transformations are computationally simplified by applying them to the coefficient vectors \mathbf{c} of the signals. In this way, the resultant torque would also be a Fourier series with $N + 1$ terms. No additional noise nor frequencies will be present in the torque obtained in that way. The result of the stress and strain transformations can be seen in Fig. 7.

Steady torque and friction force values A single friction coefficient value has to be obtained from each test run. This means that a single torque value has to be obtained. Most of the times, the torque variation in time had a single short peak (in which the system accelerates) followed by a relatively steady segment. In order to take a representative single torque value, it was decided that only the steady region would be used. Therefore, the single torque value was taken to be the average of all the values in the steady segment.

In order to obtain the torque values of the steady region, the point separating the peak from it had to be defined. A Gaussian function g was fitted to the

peak using least squares:

$$g(t) = h \cdot \exp\left(-\frac{(t-p)^2}{2\sigma^2}\right). \quad (9)$$

The peak height h and the peak location p were taken, respectively, to be the maximum torque value recorded in a given test run and the time at which this value was observed. The fitting process gives the parameter $\hat{\sigma}$ (equivalent to the standard deviation of a Gaussian probability distribution function). Furthermore, it was observed that only readings taken at times $t_i \in [p - 0.1(t_M - t_0), p + 0.1(t_M - t_0)]$ are appropriate to be used for the regression. A suitable transition point from peak to steady segment was observed to be at $t = p + 2\hat{\sigma}$. As a result, the steady torsion value was obtained from the measurements corresponding to $t_i \in [p + 2\hat{\sigma}, t_M]$. The Gaussian fitting function g and the steady segment definition are illustrated in Fig. 8.

The single steady friction force for each test run was approximated to be equal to the steady torsion value divided by the omni-wheel radius. Dynamic effects were not taken into account. A CAD model of the wheel and the shaft rendered a moment of inertia about the axis of the shaft of $4 \text{ kg}\cdot\text{cm}^2$. Considering rolling without slip requires including the Steiner term [12]. Taking that into account results in a moment of inertia of $10 \text{ kg}\cdot\text{cm}^2$. The angular acceleration values were found to be relatively low, especially in the steady region. This makes the product of angular acceleration with the moment of inertia much lower than the applied torque, in orders of 10^{-2} . That is why it was decided that the system can be approximated as static without loss in accuracy. As a result, steady friction force was taken to be equal to the steady torsion value divided by the omni-wheel radius. The friction coefficient observed for each test run can be obtained

by taking the ratio of the steady friction force to the normal force (recorded from the scale readings).

Slip ratio measurements

The relative velocity between the omni-wheel and the platform, as well as the slip ratio, are important parameters characterizing the amount of slip in a given test run. In order to obtain them, first, the potentiometer readings were smoothed and differentiated. Then, single representative values for every test run were obtained.

Combined iterative smoothening Iterative filtering was applied in order to smoothen the signals from the two potentiometers. On each iteration a Butterworth filter was used followed by a rolling average. Appropriate smoothening was observed after seven such iterations, each with different parameters.

The cutoff frequency of the applied first order low-pass Butterworth filter was different at every iteration. The cutoff frequency was decreased for each successive iteration. The last iteration had a cutoff frequency of 20 Hz. In order to mitigate the phase shift that might occur when the Butterworth filter is applied, on each iteration the filter was applied twice: once in forward (in time) direction and once in reversed direction [13]. There was also a need to reduce the inaccuracies in the ends of the signal. The further the value at an end was from zero, the more significant were the inaccuracies. That is why a line connecting the first and the last voltage reading was subtracted from the signal. In this way both ends were at zero while the smoothness of the signal was preserved. After applying the Butterworth filter (forward and in reverse) the subtracted line was added back to the signal. This procedure successively removed the noise and variations in the signal without adding new features to it.

The running average part of the combined smoothening was applied with a different number of data points. The number of data points increased with each iteration. For applying a rolling average for n data points, the n -vector $[1/n, \dots, 1/n]$ was convoluted with the signal. In order to have the same smoothening throughout the whole resultant signal, it was taken only for points at which the original signal and the n -vector $[1/n, \dots, 1/n]$ overlap completely. That resulted in a shorter (cut-off) signal at every iteration of the combined smoothening. However, together with the strategies applied to the Butterworth filter, this procedure resulted in properly smoothened ends of the signals. The results of the combined iterative smoothening can be seen in Fig. 9.

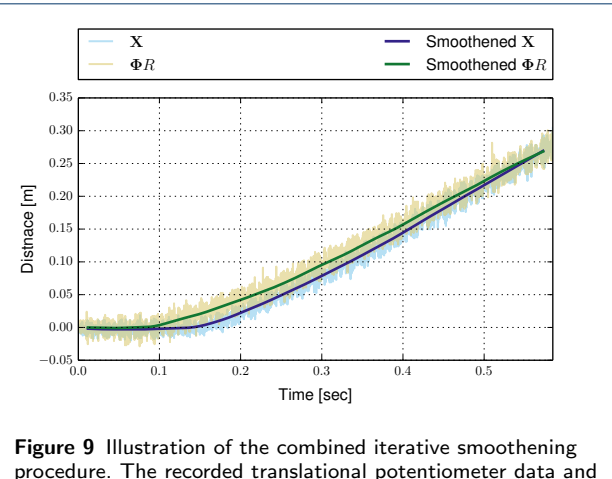


Figure 9 Illustration of the combined iterative smoothening procedure. The recorded translational potentiometer data and rotational potentiometer data multiplied by the omni-wheel radius are presented together with their smoothed counterparts

Differentiation The translational and angular velocities needed to calculate the relative velocity and the slip ratio can be obtained by differentiating the smoothed signals from both potentiometers. The differentiation was done by taking the central difference. In that way the differentiation error is reduced [14]. In particular, the differentiation scheme is:

$$V_i = \frac{X_{i+1} - X_{i-1}}{t_{i+1} - t_{i-1}}, \text{ for } i = 2, \dots, (M-1), \quad (10)$$

where X_i and V_i are respectively the translational position and the velocity of the platform at time t_i , and M is the dimension of the translational position vector \mathbf{X} . Eqn. 10 can be applied in the same way for the rotational displacement vector Φ of the wheel and its angular velocity ω . It can be seen from the definition in Eqn. 10 that the dimension of the vector \mathbf{V} is $M - 2$. That means that by differentiating, the signal gets shorter by two data points (the first and the last one).

After applying central difference differentiation, the obtained signal is also smoothed. The same combined iterative smoothening applied to the original signals is again applied to the differentiated ones. That results in further shortening of the signal. The result of the complete differentiation procedure is presented in Fig. 10.

Relative velocity and slip ratio By using the translational and rotational velocity vectors \mathbf{V} and ω , the relative velocity and the slip ratio can be obtained. The relative velocity r is defined as:

$$r = \omega R - V \quad (11)$$

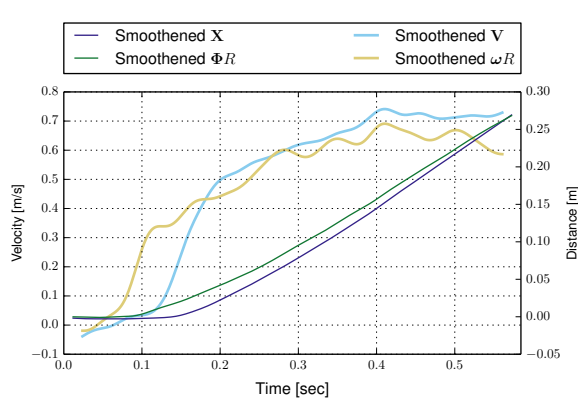


Figure 10 Illustration of the differentiation procedure results

for a given translational velocity V , rotational velocity ω and wheel radius R . The definition for slip ratio s (originally given in Eqn. 3) can be rewritten as:

$$s = \frac{\omega R - V}{V} = \frac{r}{V}. \quad (12)$$

These two parameters can be easily calculated as functions of time by applying Eqns. 11 and 12 to every pair of V_i and ω_i .

Again, similar to the case with the torque measurement, a single value for the relative velocity and the slip ratio for every test run had to be obtained. The same $p + 2\hat{\sigma}$ point defined for the torque was used as a separation point for the relative velocity and the slip ratio. The steady relative velocity and the slip ratio values were taken to be the averages of the measurements corresponding to $t_i \in [p + 2\hat{\sigma}, t_M]$. It should be noted that M is the size of the \mathbf{V} and $\boldsymbol{\omega}$. The size of \mathbf{V} and $\boldsymbol{\omega}$ would be equal if the same number of combined iterative smoothening with the same parameters is applied to both vectors.

Results

Five sets of tests were performed. Four of these sets were done with the clean wheel at angles 0° , 15° , 30° and 45° with respect to the forward movement. The fifth test was done only with the coated wheel at an angle of 0° . Each one of these sets was performed at four normal force settings corresponding to 4, 5, 6 and 8 kg. Furthermore, the voltage was set at five distinct levels. Two repetitions of every combination of test set, normal force setting and voltage level were performed. Each of these repetitions took about one minute to set and run.

The data recorded during each test was analysed as previously described and the slip ratio and friction coefficient were obtained. The results can be seen in Figs.

11 and 12. Trends can be observed despite the significant amount of noise. Furthermore, outliers are also present. The outliers are considered to be a result of erroneous readings. The maximum friction coefficient for each test set can be seen in Table 1. In the process of obtaining the values in Table 1, the outliers were not taken into account. The relationship between the maximum coefficient of friction μ_{max} and the approach angle (α) for the clean wheel can be observed in Fig. 13. A linear regression trend line is also presented. These values are within the expected range of normal rubber wheels friction coefficients on carpets [15].

During the data processing it came to light that some of the data points for the test set of the clean omni-wheel at 0° angle are erroneous due to bad clamping of the shaft and the motor. The test could not be repeated so it was decided that the data would be kept. However, in order to examine the trends between the different test sets (as in Fig. 13) only the subset of reliable data was considered for obtaining the maximum coefficient of friction μ_{max} for that test set. As a consequence, in Table 1 the value of 0.1868 is used instead of 0.5324 that can be seen in Fig. 11a. The value of 0.1868 is the highest observed among the non-erroneous tests.

In Fig. 12 the data for the coated and clean wheels at 0° angle are presented together. The effect of the coating on the friction coefficient can be observed by comparing the distribution of the two marker sets along the vertical axis. The data shown in Fig. 12 suggests that the coating results in lower value for the maximum friction coefficient μ_{max} . However, this plot also includes the erroneous data for the test set of the clean omni-wheel at 0° angle. If only the subset of reliable data and the values in Table 1 are considered, the coating results in higher value for the maximum friction coefficient μ_{max} . Furthermore, the coating endured the tests and showed no sign of wear. However, its color changed from white to beige. Possible reasons for that are oxidation, chemical reaction with the rubber rollers or a chemical process catalyzed by the heat generated from the friction.

Table 1 Maximum friction coefficient μ_{max} observed for each of the five sets of test

Test set	μ_{max}
Clean, 0°	0.1868
Clean, 15°	0.2475
Clean, 30°	0.4504
Clean, 45°	0.5861
Coated, 0°	0.4430

Discussion

Over two hundred tests were conducted in order to validate the performance of the set-up. The main aim,

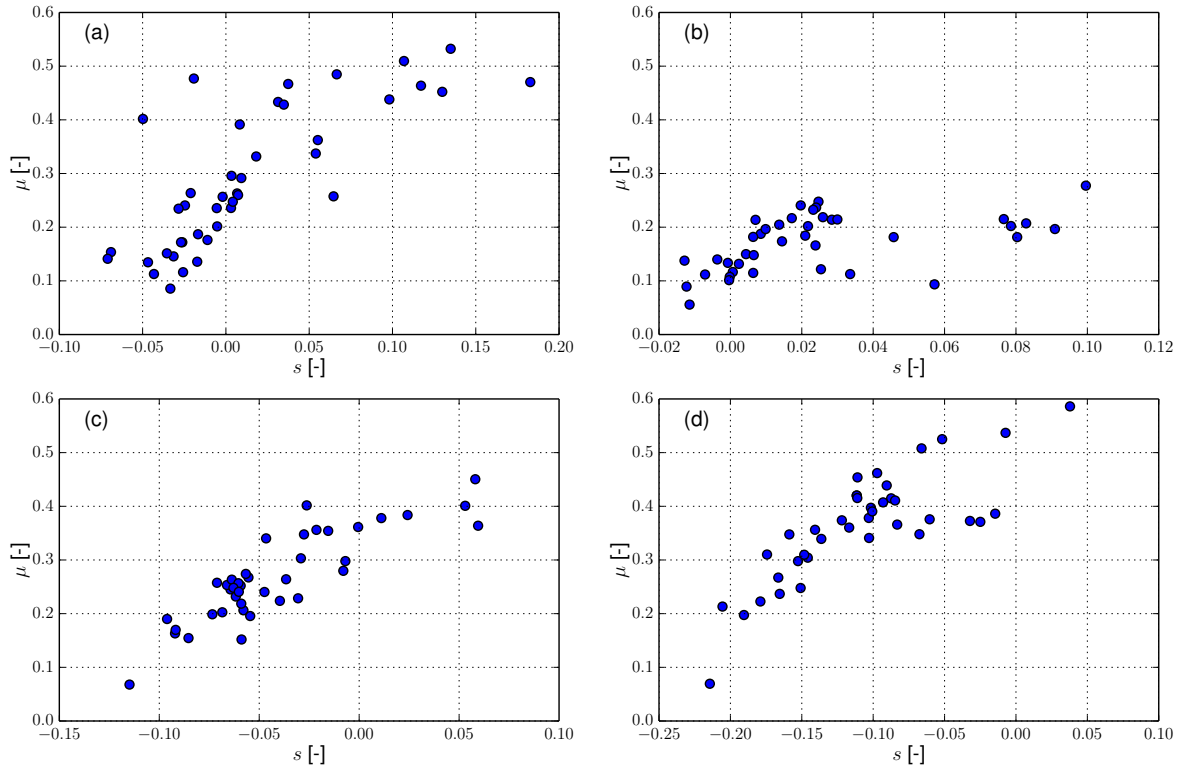


Figure 11 Plots of the obtained friction coefficient μ and slip ratio s for the clean (not coated) omni-wheel: **a** Approach angle 0° , **b** Approach angle 15° , **c** Approach angle 30° , **d** Approach angle 45°

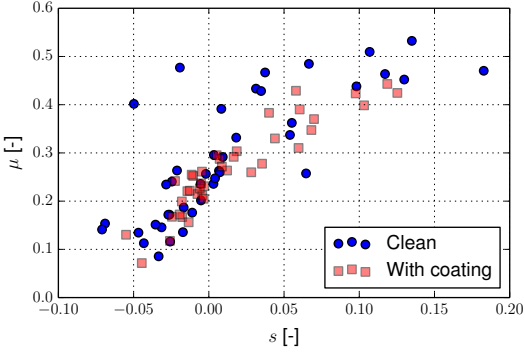


Figure 12 Comparison between the friction coefficient μ and slip ratio s for the clean and the coated omni-wheels at approach angle of 0°

being measuring the friction coefficient, is confirmed to be achieved by the use of strain gauges. As a secondary objective, the relative velocity and the slip ratio were obtained using the two potentiometers. The processed output of the DAQ made the set-up a complete tool for

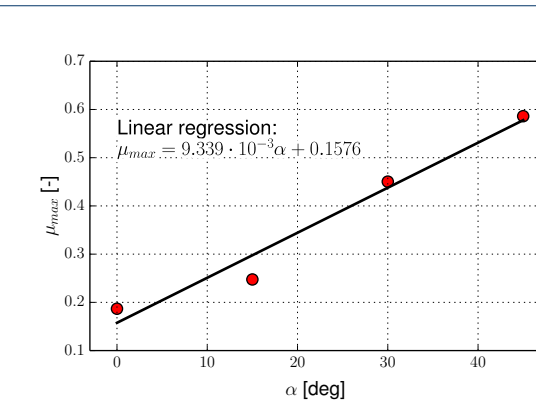


Figure 13 Relationship between approach angle α and maximum friction coefficient μ_{max} for the clean wheel

measuring the friction coefficient of the omni-wheels. The tests are illustrated in Fig. 11, where each data point represents the averaged behaviour of the omni-wheel during a run. By making possible the change of the approach angle, it is proved by our results that the friction coefficient increases with this angle (Fig. 13).

The reliability of the results consists in the precision of the sensors, instruments and the signal processing techniques that were used. The number of repetitions of a test has also a considerable effect when gathering experimental data. As only two repetitions per test were performed for the presented results, and some errors were encountered during the experimental phase, conclusions can not be drawn for the first set of tests (Fig. 11a).

The described findings discussed in the previous section suggest that the sensors and the instruments of the set-up should be improved in the future studies. Currently, the normal force is measured only at the beginning of the test due to the low frequency rate of the instrument. As the omni-wheels experience vibrations during rolling, due to the irregularities of the small rollers, the normal force is expected to oscillate. We believe that a high frequency acquisition of the weight can improve the accuracy of the tests. Also, the friction of the bearing rails of the moving platform was neglected during the experiments. This highlights another strong point for improvement in the future. Nevertheless, within the scope of the present study, the set-up proved to show the possibility of measuring the torque, the relative velocity, the normal force, and most importantly the friction coefficient of an omni-wheel.

Conclusion

As omni-wheels are often used on robot platforms, it is highly important to consider the friction force at an early stage of the design. In that way, the drive-train of the platform can be sized accordingly. This research aimed to propose a friction coefficient testing methodology suitable to be applied for omni-wheels. The presented method resulted in qualitative observations and the approach was shown to be valid. The omni-wheels were tested at different speeds, torques, normal forces and angles with respect to the forward movement. For each one of these tests a single value for the friction coefficient was obtained.

The data showed that the friction coefficient increases with the angle between rotating axis of the wheel and the forward movement. At 0° the found coefficient of friction was approximately 0.19, going up to 0.59 at the angle 45°. These values are within the expected range for normal rubber wheels.

In the future, more omni-wheels of different sizes and coatings should be tested using the same set-up. Further verification using pairs of materials with known friction coefficients has to be done. The relation between the slip and the approach angle is still to be investigated. How the wheels perform on an inhomogeneous contact surface will also be further studied.

Competing interests

The authors declare that they have no competing interests.

Acknowledgements

We would like to thank Arianne Bijma from ASML and Patrice Kauw from TU Delft for initiating this project. The equipment and working space for this project was provided by Jos Sinke and the staff of DASML at TU Delft. Special thanks are extended to Kees Paalvast for the technical assistance he provided. The authors are deeply grateful to Gawel Kuš for offering help in a hard time. Finally, guidance given by Angeniet Kam has been a great help in writing this article.

References

- Popov, V.L.: *Contact Mechanics and Friction*. Springer, Berlin, Germany (2010)
- Blau, P.J.: *Friction Science and Technology*. Marcel Dekker, Inc., New York, USA (1996)
- Goryacheva, I.G.: *Contact Mechanics in Tribology*. Kluwer Academic Publishers, Dordrecht, The Netherlands (1998)
- Rabinowicz, E.: *Friction and Wear of Materials*, 2nd edn. John Wiley & Sons, Inc., New York, USA (1995)
- Hunter, S.C.: The rolling contact of a rigid cylinder with a viscoelastic half space. *Journal of Applied Mechanics* **28**(4) (1961)
- Morland, L.W.: A plane problem of rolling contact in linear viscoelasticity theory. *Journal of Applied Mechanics* **29**(2) (1962)
- Pokorski, J., Renski, A., Sar, H.: Measurement system for investigation of tyre-road friction. In: International Scientific Conference MOSATT 2011; Koszyce, Zlata Idka
- Salaani, M., Evans, L., Harris, J., MacIsaac, J.: NHTSA Tire Rolling Resistance Test Development Project - Phase I. U.S. Department of Transportation - National Highway Traffic Safety Administration. Paper Number 09-0300
- Love, A.E.H.: *A Treatise on the Mathematical Theory of Elasticity*, 4th edn. Dover Publications, New York, USA (1944)
- Eccles, W.: *Pragmatic Electrical Engineering: Systems & Instruments*. Morgan & Claypool Publishers, San Rafael, California, USA (2011)
- Young, W.C., Budynas, R.G.: *Roark's Formulas for Stress and Strain*, 7th edn. McGraw-Hill, New York, USA (1989)
- Hibbeler, R.C.: *Statics*, 13th edn. Pearson Education, New York, USA (2013)
- Gustafsson, F.: Determining the initial states in forward-backward filtering. *IEEE Transactions on Signal Processing* **44**(4), 988–992 (1996)
- Riley, K.F., Hobson, M.P., Bence, S.J.: *Mathematical Methods for Physics and Engineering: A Comprehensive Guide*, 3rd edn. Cambridge University Press, Cambridge, United Kingdom (2006)
- Khaled, W.A.-E., Carter, J.K., Jerome, J.C., Alfred, A.A., Omer, C.J., Will, G.: Factors affecting minimum push and pull forces of manual carts. *Applied Ergonomics* **30**, 235–245 (1999)

Additional Files

Additional file 1 — rawData.zip

Raw data files as recorded by the DAQ system. File description included.